International Journal of Pharmaceutics 403 (2011) 1–14

Contents lists available at ScienceDirect

International Journal of Pharmaceutics

journal homepage: www.elsevier.com/locate/ijpharm

Velocity profiles and shear strain rate variability in the USP Dissolution Testing Apparatus 2 at different impeller agitation speeds

Ge Bai[1], Yimin Wang, Piero M. Armenante*

Otto H. York Department of Chemical, Biological and Pharmaceutical Engineering, New Jersey Institute of Technology, Newark, NJ 07102, USA

ARTICLE INFO

Article history:
Received 28 June 2010
Received in revised form
21 September 2010
Accepted 22 September 2010
Available online 29 September 2010

Keywords:
Dissolution testing
USP Dissolution Testing Apparatus 2
Hydrodynamics
Computational Fluid Dynamics (CFD)
Laser Doppler Velocimetry (LDV)
Agitation speed
Velocity profiles
Shear strain rate

ABSTRACT

The fluid velocity profiles at different locations inside a standard USP Dissolution Testing Apparatus 2 were experimentally obtained via Laser Doppler Velocimetry (LDV) at three impeller agitations speeds, namely 50 rpm, 75 rpm and 100 rpm. The experimental results were compared with the predictions obtained with Computational Fluid Dynamics (CFD) where the κ–ω model with low Reynolds number correction was used to account for turbulence effects. In general, good agreement was found between the experimental LDV velocity measurements and the CFD simulation predictions. The non-dimensional tangential, axial and radial velocity profiles (scaled with the impeller tip speed) and the flow pattern were found to be nearly independent of the agitation speed in most regions of the vessel, implying that increasing the agitation speed generally produced a corresponding increase in the local values of the velocity. However, the velocity profiles and flow pattern in the inner core region just below the impeller, where the dissolving tablet is usually located, were found to be much less sensitive to agitation speed. In this region, the axial and radial velocities were especially low and were not significantly affected by agitation increases. This inner core region at the center of the vessel bottom persisted irrespective of agitation intensity. The CFD predictions also indicated that increasing the agitation speed resulted in a higher shear strain rate distribution along the vessel bottom, although the strain rate was always very low at the center of the vessel bottom, even when the agitation speed was increased.

1. Introduction

In the pharmaceutical industry, drug dissolution testing is routinely used to provide critical *in vitro* drug release information for both quality control purposes, i.e., to assess batch-to-batch consistency of solid oral dosage forms such as tablets, and drug development, i.e., to predict *in vivo* drug release profiles. Several dissolution apparatuses exist. They are standardized and specified in the United States Pharmacopoeia (USP) (United States Pharmacopeia, 2008). Among these apparatuses, the most widely and commonly used is the UPS Dissolution Testing Apparatus 2, simply referred to in this document as "Apparatus 2".

In vitro dissolution data generated from dissolution testing experiments can be related to *in vivo* pharmacokinetic data by means of *in vitro–in vivo* correlations (IVIVC). A well established predictive IVIVC model can be very helpful for drug formulation design and post-approval manufacturing changes (Kortejärvi et al., 2006). The main objective of developing and evaluating an IVIVC is to establish the dissolution test as a surrogate for human bioequivalence studies, as stated by the Food and Drug Administration (FDA). According to Qureshi and Shabnam (2001), "Considering the usefulness of drug dissolution testing, regulatory agencies and pharmaceutical manufacturers are suggesting an enhanced role for such testing towards expeditious approval and economical availability of drug products on the markets. That is, more extensive drug dissolution testing (e.g. use of different media, drug release profiles rather than single point testing) could be sufficient without *in vivo* testing, in many cases, to establish safety and efficacy of a drug product following minor formulation and manufacturing changes." However, for this to happen, but also to insure that the current dissolution testing method is a robust method, the dissolution testing apparatus used to conduct dissolution tests must be able to provide accurate and reproducible results.

Apparatus 2 has been used in the pharmaceutical industry for decades since it was first officially introduced almost 40 years ago (Cohen et al., 1990). However, dissolution testing using Apparatus 2 remains susceptible to significant error and test failures. Several reports in the literature have suggested that there is considerable variability, unpredictability and randomness in dissolution profiles using Apparatus 2 (Cox and Furman, 1982; Cox et al., 1983;

* Corresponding author at: New Jersey Institute of Technology, Otto H. York Department of Chemical Engineering, 323 M.L. King Boulevard, Newark, NJ 07102-1982, USA. Tel.: +1 973 596 3548; fax: +1 973 596 8436.
E-mail address: piero.armenante@njit.edu (P.M. Armenante).
[1] Current address: MedImmune LLC, One MedImmune Way, Gaithersburg, MD 20878, USA.

0378-5173/$ – see front matter © 2010 Elsevier B.V. All rights reserved.
doi:10.1016/j.ijpharm.2010.09.022

Nomenclature

D	impeller diameter (m)
k	turbulence kinetic energy ($m^2\ s^{-2}$)
g_i	body force in the i direction per unit mass ($m\ s^{-2}$)
G_k	generation of k due to mean velocity gradients ($kg\ m^{-1}\ s^{-3}$)
G_ω	Generation of ω ($kg\ m^{-3}\ s^{-2}$)
N	impeller rotational speed (rotations/s)
r	radial coordinate of LDV measurement point (m or mm)
P	pressure (N/m^2)
$\bar{P}$	local average pressure (N/m^2)
Re	impeller Reynolds number ($=\rho ND^2/\mu$) (dimensionless)
$\mathbf{S}$	rate-of-deformation tensor (s^{-1})
S_{ij}	component of the rate-of-deformation tensor (s^{-1})
S_k	user-defined source term of k ($kg\ m^{-1}\ s^{-3}$)
S_ω	user-defined source term of ω ($kg\ m^{-3}\ s^{-2}$)
t	time (s)
T	vessel diameter (m or mm)
U_i	velocity in the i direction ($m\ s^{-1}$)
U_i'	fluctuating component of the velocity in the i direction ($m\ s^{-1}$)
$\overline{U}_i$	time-average velocity magnitude in the i direction ($m\ s^{-1}$)
U_{axial}	fluid velocity in the axial (vertical) direction ($m\ s^{-1}$)
U_{radial}	fluid velocity in the radial direction ($m\ s^{-1}$)
$U_{tangential}$	fluid velocity in the tangential direction ($m\ s^{-1}$)
U_{tip}	velocity of the impeller tip ($m\ s^{-1}$)
x_i, x_j	coordinates in the i and j directions
Y_k	dissipation of k ($kg\ m^{-1}\ s^{-3}$)
Y_ω	dissipation of ω ($kg\ m^{-3}\ s^{-2}$)
z	vertical location of iso-surface (m or mm)

Greek symbols

$\dot{\gamma}$	magnitude of strain rate (s^{-1})
Γ_k	effective diffusivity of k ($kg\ m^{-1}\ s^{-1}$)
Γ_ω	effective diffusivity of ω ($kg\ m^{-1}\ s^{-1}$)
ε	turbulent dissipation rate ($m^2\ s^{-3}$)
μ	liquid viscosity ($kg\ m^{-1}\ s^{-1}$)
ρ	liquid density ($kg\ m^{-3}$)
$\boldsymbol{\tau}$	stress tensor ($kg\ m^{-1}\ s^{-2}$)
ω	specific dissipation rate (s^{-1})

Bocanegra et al., 1990; Moore et al., 1995; Qureshi and McGilveray, 1999; Costa and Lobo, 2001; Qureshi and Shabnam, 2001; Mauger et al., 2003) even when dissolution apparatus calibrator tablets are used (Cox and Furman, 1982; Moore et al., 1995; Qureshi and Shabnam, 2001; Kukura et al., 2003; Baxter et al., 2005).

Earlier studies (McCarthy et al., 2003, 2004; Kukura et al., 2004; Baxter et al., 2005) including publications by this group (Bai et al., 2007a; Bai and Armenante, 2008, 2009) have indicated that the complex hydrodynamics that can be observed in Apparatus 2 can contribute to the poor reproducibility and data inconsistencies that can be obtained with this apparatus. Under the typical operating conditions used in this test, the fluid flow in Apparatus 2 is highly heterogeneous. Hence this system can be expected to be associated with a complex hydrodynamics, resulting in fluid velocities whose directions and intensities are highly dependent on the location within the vessel, especially at the bottom of the vessel where the tablet is located during dissolution testing.

A literature review shows that only a limited number of hydrodynamic studies have been conducted on Apparatus 2 over the past 30 years. The first Laser Doppler anemometry (LDA) measurements of the velocities in Apparatus 2 were reported by Bocanegra et al. (1990). However, the data they obtained were only generated in very limited regions of the vessel. More recently, qualitative flow patterns were obtained using Particle Image Velocimetry (PIV) and Laser-Induced Fluorescence (LIF). The flow patterns were compared to the velocity flow field simulated using Computational Fluid Dynamics (CFD) (Kukura et al., 2003). Other researchers also made efforts to determine the flow field inside the USP Dissolution Test Apparatus 2 vessel through CFD (Kukura et al., 2004; Baxter et al., 2005). However, the CFD simulations mentioned above were only qualitatively validated against experimental data. McCarthy et al. (2003, 2004) predicted the flow field with CFD and compared the CFD predictions with the limited experimental results from previous research (Bocanegra et al., 1990).

In previous work by this research group (Bai et al., 2007a), the velocity field throughout Apparatus 2 was quantified via Laser Doppler Velocimetry (LDV), and CFD computer simulations were used to predict the three-dimensional flow in Apparatus 2 in order to validate the simulation predictions against the experimental LDV data. Thus, a complete spectrum of flow field information including velocity magnitude and direction, turbulence kinetic energy, energy dissipation rate and shear strain rate predicted by CFD simulation was used to quantify the hydrodynamics of Apparatus 2 with confidence (Bai et al., 2007a). In addition, this validated CFD model was applied to study the mixing efficiency of Apparatus 2 by predicting the system mixing time under different impeller agitation speeds (Bai et al., 2007b). This study showed that the drug released by the tablet during the dissolution process is transported to the sampling point higher in the vessel relatively quickly (on the order of 30 s at 50 rpm). Further studies have additionally shown that small changes in the geometry of the system can produce large effects on the system hydrodynamic and the dissolution profiles. For example, the velocity flow field and the shear strain rate near the vessel bottom are dramatically impacted by small misalignments of the impeller location (Bai and Armenante, 2008). Similarly, the exact location of the tablet during the dissolution process can result in very different dissolution profiles which may result in failure to pass the acceptance criteria established by the FDA (Bai and Armenante, 2009).

The impeller agitation speed is a key variable in *in vitro* dissolution testing with Apparatus 2 since it affects the velocity in the vicinity of the tablets and hence the tablet–liquid mass transfer rate, the rate of drug release, and the dissolution curve. If disintegrating tablets are used, the agitation speed additionally controls whether the tablet fragments accumulate under the impeller ("coning" effect) or become suspended in the liquid (Ross and Rasis, 1998; Qureshi and Shabnam, 2001, 2003; Bai et al., 2007a).

The impeller agitation speed generally recommended for Apparatus 2 is 50 rpm (Shah et al., 1992; FDA, 1997). However, in the industrial practice, agitation speeds ranging from 50 to100 rpm are commonly used, with 25 rpm and 150 rpm also been employed, although more rarely, depending on the tablet and the drug product being tested (Gibaldi and Feldman, 1967; Cox et al., 1983; Costa and Lobo, 2001; Kamba et al., 2003). In all cases, the ultimate goal of the way the dissolution test is conducted and the agitation speed is selected is to "allow maximum discriminating power and to detect products with poor *in vivo* performance" (Fruitwala et al., 1998).

Although there is now quantitative information to understand the hydrodynamics in dissolution vessels stirred at 50 rpm, much more limited information is available on the hydrodynamics of Apparatus 2 when the impeller agitation speed is higher than 50 rpm. Bocanegra et al. (1990) applied LDA to measure velocities in Apparatus 2 in selected regions for an agitation speed of 60 rpm, which is a rarely used agitation speed in practice. Kukura et al. (2004) simulated the flow field in Apparatus 2 with CFD and

Table 1
Dimensions of impeller and shaft.

Component of impeller or shaft	Dimension (mm)
Shaft diameter	9.53
Length of top edge of impeller blade	74.10
Length of bottom edge of impeller blade	42.00
Height of impeller blade	19.00
Thickness of impeller blade	5.00

predicted the shear strain rate at an agitation speed of 100 rpm, although their modeling results were not compared with experimental results in a quantitative fashion. Finally, McCarthy et al. (2004) studied the hydrodynamics in Apparatus 2 at 25, 100 and 150 rpm with a partially validated CFD model (McCarthy et al., 2003). Hence, there is a need for experimentally quantifying and computationally predicting the hydrodynamics of Apparatus 2 at agitations speed higher than 50 rpm.

Therefore, in the present work, LDV velocity measurements were collected in Apparatus 2 at agitation speeds of 50, 75 and 100 rpm and a CFD model previously validated at 50 rpm (Bai et al., 2007a) was used here to predict the fluid field at these agitation speeds. The results of the CFD simulations were then compared the LDV data to validate the computational approach. Finally, CFD-based predictions of shear strain rate, the driving force of dissolution, were made as well.

2. Experimental apparatus and method

2.1. Dissolution vessel and agitation system

A standard USP Dissolution Testing Apparatus 2 vessel consisting of an unbaffled, cylindrical, hemispherical-bottomed, glass vessel with a prescribed maximum nominal volume of 1 L was used (*remark*: unlike most cylindrical vessels used in industry, Apparatus 2 is "unbaffled", meaning that it does not contain "baffles", i.e., rectangular vertical plates (typically four) commonly placed next to the cylindrical wall of vessels and reactors, and used to dissipate energy, reduce the tangential component of the fluid velocity in the vessel, and promote axial (vertical) fluid recirculation, in order to achieve a more uniform distribution of fluid velocities in the vessel). The vessel diameter was measured with a caliper and was found to be 100.16 mm. The vessel was placed in a square Plexiglas tank filled with water in order to minimize refractive effects at the curved surface of the vessel wall during the LDV measurements. The agitation system consisted of a standard Apparatus 2 two-blade paddle. The exact geometries of the impeller and shaft, also measured with a caliper, are listed in Table 1. The impeller was centrally mounted in the vessel and was placed 25 mm off the vessel bottom, as specified in the USP, using a HeighChek Distek® tool, which can accurately set the paddle clearance off the vessel bottom prior to a test. 900 mL of de-ionized water was added to the dissolution vessel, as prescribed by the USP. The temperature of the water was maintained at room temperature ($25 \pm 1\,^{\circ}C$). An electric motor connected to an external controller was used to rotate the impeller clockwise at three agitation speeds, i.e., 50, 75, and 100 rpm, corresponding to impeller tip speeds of 0.194 m s^{-1}, 0.291 m s^{-1} and 0.388 m s^{-1}, respectively. The corresponding impeller Reynolds numbers were 4939, 7409, and 9878.

A small amount of silver-coated hollow borosilicate glass spheres (Dantec Measurements Technology USA, Mahwah, NJ, USA) with a density of 1.4 g/cm^3 was added to the water as seed particles. The particle size ranged from 2 to 20 μm with a mean size of 10 μm. These glass spheres were used to follow the fluid flow and scatter the laser light used in the LDV fluid velocity measurements.

In additional experiments, a millimeter scale was taped to the shaft, the vessel was filled with 900 mL of water, and the level of the water–air interface was measured at rest against this relative scale. The level of the same interface at the shaft was then measured at different agitation speeds by taking photographs from above the liquid surface in order to determine the change in liquid level near the shaft caused by the agitation-induced vortex.

2.2. Laser Doppler Velocimetry (LDV) system

A Laser Doppler Velocimetry (LDV) apparatus (Dantec Measurement Technology USA, Mahwah, NJ, USA) was used to experimentally measure, non-intrusively, the fluid velocities at selected points inside the dissolution vessel (Fig. 1).

The LDV system consisted of single-color, two-beam Dantec 55X series backscatter LDV apparatus. A 750 mW argon-ion laser (Ion Laser Technology, Inc.) produced a single multicolored laser beam, which was passed through an optical filter to generate a monochromatic green beam (wavelength: 512 nm). This beam passed through a beam splitter from which two beams emerged, one of which was passed through a Bragg cell to lower the frequency by 40 MHz and be able to distinguish between positive and negative velocity measurements. Each beam then traveled via a fiber optic cable to a probe containing a beam expander system and a final focusing lens with a focal length of 330 mm. The beams were converged inside the vessel to obtain a finite control volume formed by their intersection. The scattered light from the seed particles moving through the control volume was collected by a receiver located inside the probe, and the Doppler shift (directly proportional to the particle velocity) was measured with a photomultiplier assembly. A data acquisition system connected to a computer converted the Doppler shifts into velocity values, and produced on-line measurements of average and fluctuating velocities.

The dissolution testing system was mounted on an x–y–z traversing system that could position the vessel at any desired location in front of the LDV probe. The beams were made to converge inside the vessel, thus enabling the fluid velocity to be measured at any desired location in the dissolution vessel. The time interval for each measurement was typically 60 s. In most cases, some 600–2500 instantaneous velocity data points were collected at any location and for the selected velocity component, from which the local average velocity could be calculated. Appropriate rotation of the fiber optic probe and translation of the dissolution testing system assembly yielded the velocity components in all three directions at any location where a measurement was taken. Triplicate experiments were conducted for each velocity component at each location. The standard deviation was typically 0.001 m s^{-1}. Additional details of the methodology are provided elsewhere (Bai et al., 2007a).

In order to fully quantify the fluid flow in the dissolution system, eight horizontal surfaces (iso-surfaces) were selected inside the vessel, as shown in Fig. 2. The horizontal plane where the cylindrical and the hemispherical walls of the vessel meet was defined as z 0 mm. Two of the iso-surfaces were located above the impeller ($z = 25$ mm, $z = -0.75$ mm), three in the impeller region ($z = -6.75$ mm, $z = -15.75$ mm, $z = -25.75$ mm), and the other three below the impeller ($z = -31.75$ mm, $z = -37.75$ mm, $z = -43.75$ mm). On each iso-surface, LDV velocity measurements were taken at a number of radial positions, 5 mm apart, starting at the vessel vertical centerline (or the impeller shaft) and progressing toward the vessel wall. Typically, this resulted in eight velocity measurements being taken on each iso-surface, except for the iso-surfaces in the impeller region where velocity measurements could only be obtained in the gap between the tip of the passing blade and the vessel wall. Additionally, it was not always possible to take LDV data when the measurement location was too close to the shaft

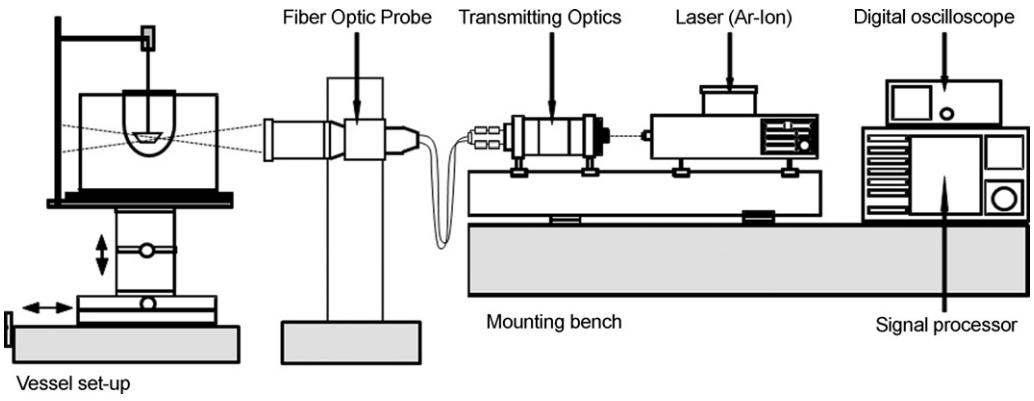

Fig. 1. Laser-Doppler Velocimetry (LDV) system used in this work.

(since the shaft reflected the light and made accurate measurements impossible), or when the curvature of the vessel made it too difficult to collect axial and radial velocities very close to the vessel wall. In such cases, no experimental LDV measurements could be taken.

3. Numerical CFD simulation

A commercial mesh generator, Gambit 2.1.6, and a computational fluid dynamic (CFD) package, Fluent 6.2.16, were used to define the computational domain, generate the grid, and numerically predict the velocity vector and velocity magnitudes at each location, as well as the turbulence level inside the Apparatus 2 vessel. In other terms, CFD was used to predict the intensity and direction of the velocity at any location inside the vessel (velocity vector field), as well as the absolute scalar value of the local velocity (velocity magnitude) at any point.

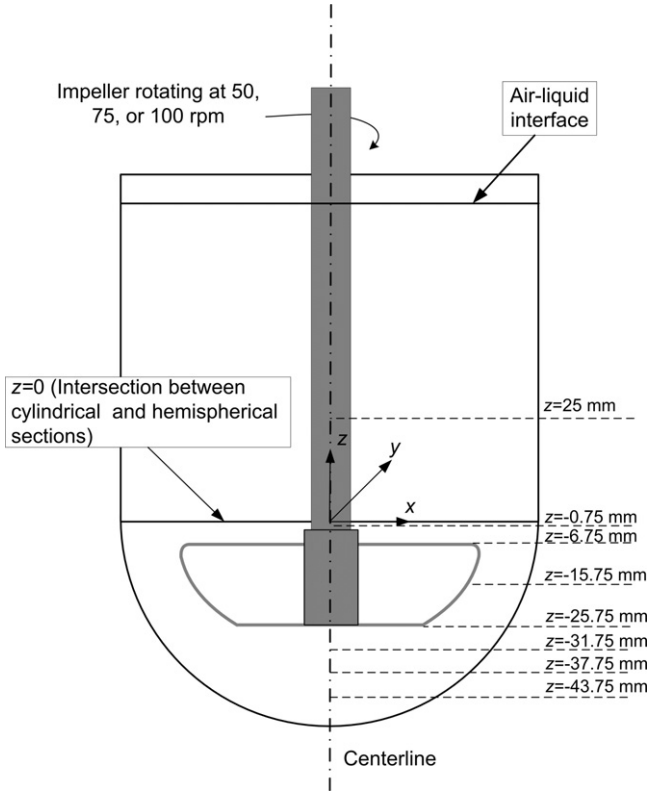

Fig. 2. Iso-surfaces where LDV measurements were taken.

The exact system geometry was used as input in Gambit to generate the mesh used in the simulations. However, as in previous work by this group, the geometry of the impeller was slightly different from that of the impeller used in the experiments in that the impeller had a slightly larger diameter shaft at the blade, resembling a collar, as opposed to the uniform shaft diameter, including the portion at the blade, typical of the USP design. The radius of this collar was only 1.6 mm larger than that of the rest of the shaft. The geometric differences between this system and the typical USP system used in the experiments are so minimal that the result obtained here is expected to be equally valid for the USP impeller with no collar. Additional details are provided elsewhere (Bai et al., 2007a,b; Bai and Armenante, 2008, 2009).

A structured Cooper-type hex mesh was created in the cylindrical portion of the vessel and in the upper section of the hemispherical bottom. An unstructured tetrahedral mesh was generated in the lower section of the hemispherical bottom of the vessel to follow the curved shape more closely. The average EquiAngle Skew parameter ranged from 0.3 to 0.4, indicating a high mesh quality. The mesh typically contained some 80,000 cells, 220,000 faces, and 63,000 nodes. Simulations with meshes containing up to some 260,000 cells were also conducted. The CFD results were shown to be mesh-independent. Additional details about the mesh and the mesh generation are provided elsewhere (Bai et al., 2007a).

CFD programs such as Fluent numerically solve the general equations representing the conservation of mass and momentum. In Cartesian coordinates, the time-averaged continuity equation for an incompressible fluid written using the summation convention can be written as:

$$\frac{\partial \bar{U}_i}{\partial x_i} = 0 \tag{1}$$

and the time-averaged momentum equation, which can be used for the prediction of the velocities in turbulent flow, is:

$$\frac{\partial \bar{U}_i}{\partial t} + \bar{U}_j \frac{\partial \bar{U}_i}{\partial x_j} = -\frac{1}{\rho}\frac{\partial \bar{P}}{\partial x_i} + \nu \nabla^2 \bar{U}_i + g_i - \frac{\partial}{\partial x_j}(\overline{U_i' U_j'}) \tag{2}$$

The last term in this equation represents the Reynolds stresses, containing the product of the fluctuating velocity components. The Reynolds stresses cannot be predicted from first principles, and they are typically calculated by making some assumptions about their relationship with other variables (closure problem). Since the flow in Apparatus 2 vessel is typically in the transitional/turbulent regimes (i.e., the flow in the dissolution system may not be fully turbulent even when operated at an impeller agitation speed of 100 rpm), a mathematical model capable of representing the turbulent instabilities in this regime is needed in order to solve the momentum equations in the CFD simulations. In previous work by our group (Bai et al., 2007a), it was shown that simulations using

the κ–ω turbulence model with low Reynolds number correction produced velocity predictions that were in closer agreement with the experimental LDV data than predictions based on other models, such as the laminar mode and RNG κ–ε model. Therefore, in this work, CFD simulations were conducted using exclusively the κ–ω model with low Reynolds number correction. The governing equations for the standard k–ω model are as follows (Bai et al., 2007a):

$$\frac{\partial}{\partial t}(\rho k) + \frac{\partial}{\partial x_i}(\rho k U_i) = \frac{\partial}{\partial x_j}\left(\Gamma_k \frac{\partial k}{\partial x_j}\right) + G_k - Y_k \quad (3)$$

$$\frac{\partial}{\partial t}(\rho \omega) + \frac{\partial}{\partial x_i}(\rho \omega U_i) = \frac{\partial}{\partial x_j}\left(\Gamma_\omega \frac{\partial \omega}{\partial x_j}\right) + G_\omega - Y_\omega \quad (4)$$

The boundary conditions used in the simulations were the same as those used previously (Bai et al., 2007a): the no-slip condition was assumed at all solid surfaces including the vessel wall, vessel bottom, and the impeller; the air–liquid interface was assumed to be flat and was modeled as a frictionless surface; and the normal gradients of all variables were zero at this interface. The appropriateness of the flat-interface assumption was determined experimentally by measuring the depth of the liquid near the shaft at different agitation speeds, as mentioned in the previous section. The results confirmed that the surface was nearly flat, as further detailed in Section 4.

The shear stress tensor, $\boldsymbol{\tau}$, is related to the rate-of-deformation tensor, $\mathbf{S}$, through the equation:

$$\boldsymbol{\tau} = -\mu \mathbf{S} \quad (5)$$

where μ is the fluid viscosity. For an incompressible Newtonian fluid, the components of the rate-of-deformation tensor, S_{ij}, are given by (Bird et al., 2002):

$$S_{ij} = \frac{\partial U_i}{\partial x_j} + \frac{\partial U_j}{\partial x_i} \quad (6)$$

Then, the local value of magnitude of the strain rate (or simply "strain rate"), $\dot{\gamma}$, is defined as:

$$\dot{\gamma} = |S| = \sqrt{\frac{1}{2}\sum_i \sum_j S_{ij}^2} \quad (7)$$

The strain rate represents the rate at which the velocity varies with distance when moving away from the point of interest.

A single reference frame approach was used in all CFD simulations. Additional details about the simulation approach are given elsewhere (Bai et al., 2007a).

4. Results

The change in liquid level near the impeller shaft at different agitation speeds with respect to the same level observed with the impeller at rest was measured by taking photographs at different agitation speeds. The liquid level at the shaft was found to drop by approximately 0 mm, 1 mm, and 2.3 mm, when compared to the liquid at rest, at agitation speeds equal to 50 rpm, 75 rpm, and 100 rpm, respectively. These level drops correspond to about 0%, 1%, and 2.3% of the vessel diameter. Furthermore, visual observations showed that this drop is not linear across the surface, but it is primarily concentrated in the neighborhood of the shaft, where the vortex is stronger, implying that most of the liquid surface is nearly perfectly flat for all practical purposes. This observation additionally implies that the assumption made for the boundary conditions used in the numerical simulations, i.e., that the liquid level is flat at all the agitation speeds tested in this work, is indeed appropriate.

4.1. Velocity profiles on iso-surfaces

Figs. 3–5 show, respectively, the tangential, axial, and radial fluid velocity profiles on all eight horizontal iso-surfaces obtained using both LDV measurements and CFD simulations at three impeller agitation speeds, i.e., 50 rpm, 75 rpm and 100 rpm, respectively. In these figures, the ordinates represent the normalized non-dimensional fluid velocity (scaled by using the impeller tip speed, U_{tip}) and the abscissas represent the normalized radial position (scaled using the vessel radius, $T/2$). It should be remarked that the scales in these figures are different depending on the velocity direction, since the tangential velocity components are typically one or even two orders of magnitude larger than the axial and radial components.

4.1.1. Velocity profiles above the impeller

Fig. 3 shows that all the tangential velocities above the impeller (iso-surfaces at $z = -0.75$ mm and $z = 25$ mm) are in same direction of the impeller rotation (all positive values). The LDV data show that on both iso-surfaces, and for all agitation speeds, the tangential velocities increase from near zero at the impeller shaft to peak values which are about 40% of impeller tip speed at similar radial positions ($0.4 < 2r/T < 0.5$). The LDV tangential velocity data remain nearly flat in the region $0.5 < 2r/T < 0.9$. When LDV measurements were taken very close to the vessel wall ($2r/T = 0.98$), the tangential velocities dropped to below 30% of the impeller tip speed on the iso-surface at $z = 25$ mm and to about 10% (50 rpm) to 15% (100 rpm) on the iso-surface at $z = -0.75$ mm, which is what one would expect since the velocity at the wall must be zero. This figure also shows that the CFD predictions match the LDV measurements quite satisfactorily in the region $2r/T < 0.4$. In the region of $0.4 < 2r/T < 0.9$, CFD simulations slightly over-predict the tangential velocities. The over-prediction increases as impeller agitation speed increases.

In the region for which $2r/T < 0.3$, the axial velocities are very small and negative above the impeller, irrespective of agitation speed (Fig. 4). On the iso-surfaces at $z = 25$ mm, and $z = -0.75$ the axial velocities are negative (downward flow) for $2r/T < 0.7$–0.8, while an upward flows occurs when $2r/T > 0.7$–0.8 for all three impeller agitation speeds. This type of flow is qualitatively similar to that observed with axial impellers in baffled system, although the intensity of the velocities is very weak here.

Finally, Fig. 5 shows that radial velocities in the region above the impeller are extremely low compared to the other two velocity components. For example, the highest value of radial velocity on the iso-surface at $z = -0.75$ mm was experimentally found to be about 1.2% of the impeller tip speed and the highest value of the radial velocity on the iso-surface at $z = 25$ mm was found to be 0.26% of the impeller tip speed irrespective of the impeller agitation speed. The differences between the LDV measurements and CFD simulation results are typically small. Considering the small scale of the velocity values of the radial velocities on these two iso-surfaces, the agreement is very good.

4.1.2. Velocity profiles in the impeller region

Because of the small gap between the rotating impeller and the vessel wall, only a limited number of LDV velocity measurements could be collected in this region, i.e., on the iso-surfaces at $z = -6.75$ mm (top edge of the impeller), $z = -15.75$ (middle of the impeller) and $z = -25.75$ mm (bottom edge of the impeller), as shown in Fig. 2.

Fig. 3 shows that in the impeller region, the tangential velocity magnitude for all three impeller agitation speeds follows same pattern, i.e., higher close to the impeller and lower close to the vessel wall. The LDV measurements show that the non-dimensional

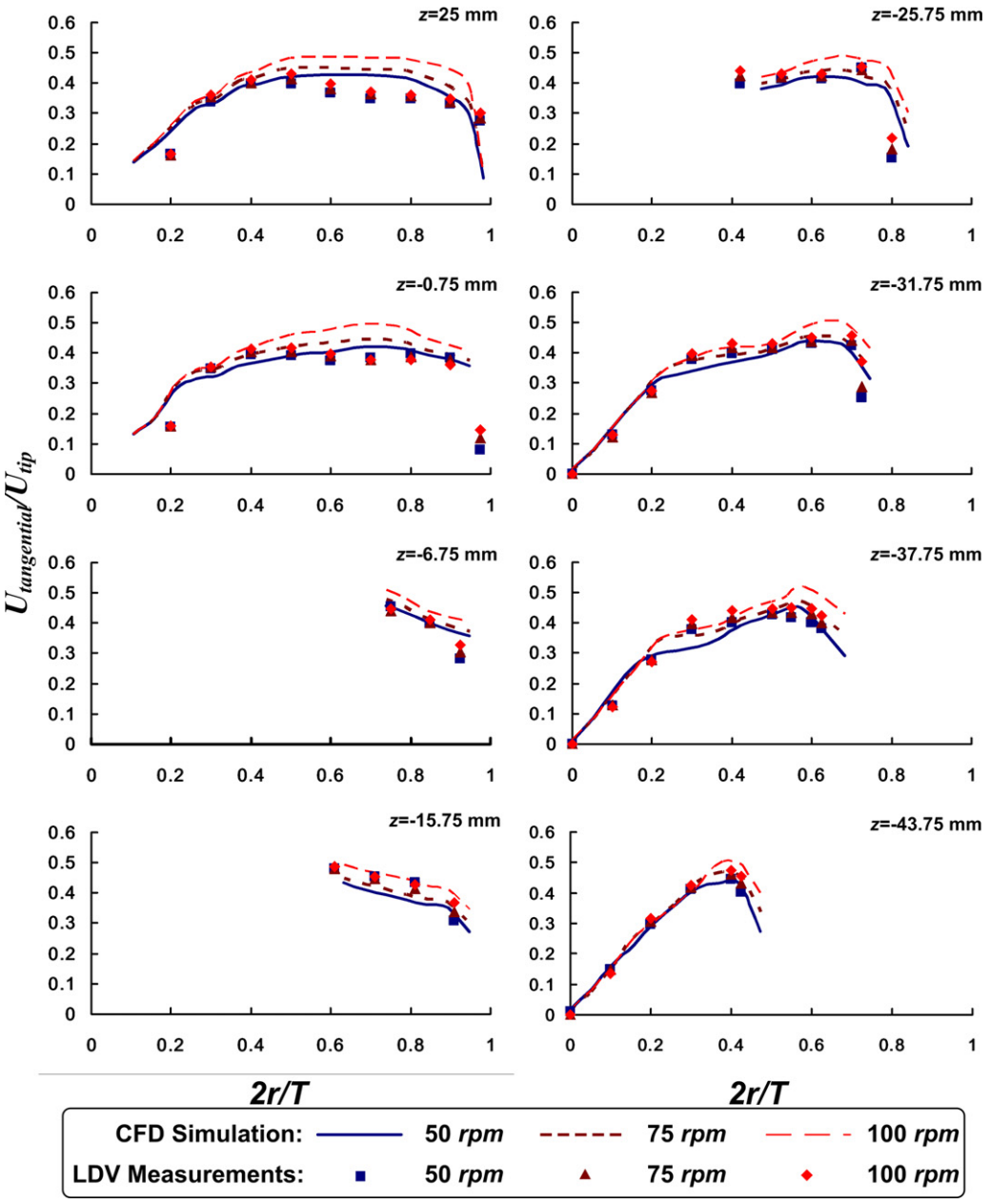

Fig. 3. Comparison between LDV data and CFD predictions for tangential velocities on different iso-surfaces at agitation speeds of 50, 75 and 100 rpm.

tangential velocity profiles do not change with increasing impeller agitation speeds except for measurements close to the wall or next to the impeller. However, even in these cases the changes are small. On the other hand, the CFD simulations predict larger differences between the profiles at different agitation speeds: the higher the speed, the higher the non-dimensional tangential velocity. However, these differences are still small, and the overall agreement between the LDV measurements and CFD simulations is still significant.

In Fig. 4, the LDV measurements for the iso-surface at $z = -6.75$ mm show that the non-dimensional axial velocity increases rapidly with radial distance, irrespective of impeller speed, thus generating an upwards flow next to the wall. However, even the highest experimental velocity was found to be only 11% of impeller tip speed, i.e., much smaller than the corresponding tangential velocity. On this iso-surface, the CFD simulations also predict an upward flow near the vessel wall, although the values of the non-dimensional velocity change more significantly with agitation speed than what was found experimentally. On the iso-surface at $z = -15.75$ mm, the non-dimensional axial velocities from LDV measurements are very small (no more than 5.2% of the impeller tip speed) for all three impeller agitation speeds, but now they start being directed downward. However, the near-zero value of these velocity for nearly all $2r/T$ values indicates that this iso-surface is very close to the horizontal plane where the horizontal jet generated by the impeller is split upwards and downwards after hitting the vessel wall (stagnation point). The CFD simulations show a similar flow pattern on this iso-surface although the predicted axial velocities are higher in absolute value than the LDV measurements in the region of $0.85 < 2r/T < 0.95$. Clearly, even a small difference between the experimental z value of the stagnation point at the wall and corresponding z value predicted computationally may result in significant discrepancies between the experimental axial velocity profiles and the corresponding CFD predictions. Finally on the iso-surface at $z = -25.75$ mm (lower edge of the impeller blade) the LDV measurements turn from minimally positive (for $0.4 < 2r/T < 0.7$) to

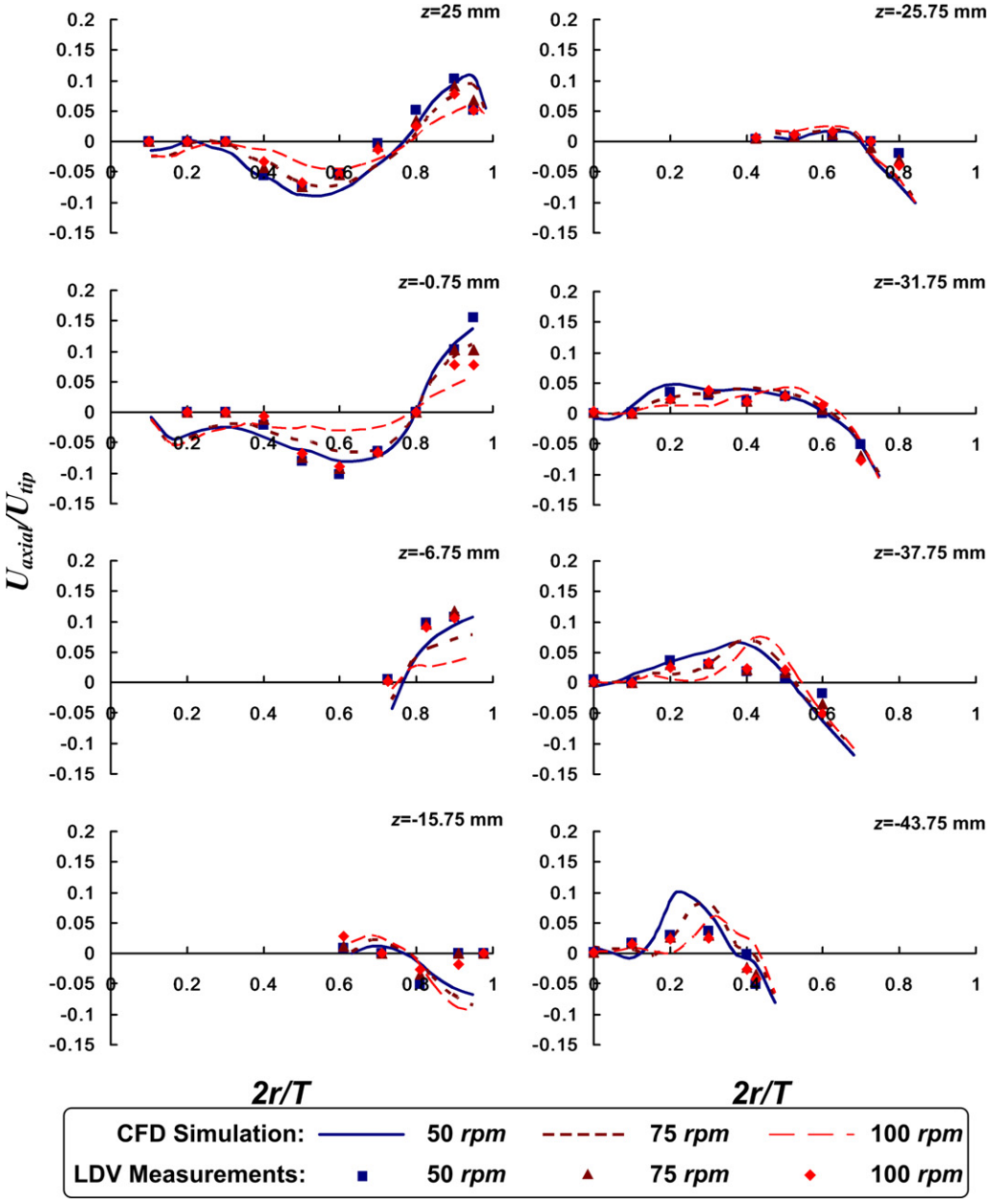

Fig. 4. Comparison between LDV data and CFD predictions for axial velocities on different iso-surfaces at agitation speeds of 50, 75 and 100 rpm.

appreciably negative (for $2r/T > 0.7$) indicating a stronger downwards flow next to the vessel wall. The impeller agitation speed has almost no impact on the non-dimensional axial velocities profiles, and the CFD predictions match the LDV measurements relatively well.

Fig. 5 shows that only a limited number of LDV measurements could be collected on the three iso-surfaces in the impeller region. This was primarily caused by the combination of a narrow gap between the edge of the impeller blade and the vessel wall and the curvature of the vessel in this region, which made radial velocity measurements much more difficult to take than for the tangential or axial velocity cases, especially near the wall. The LDV measurements were all found to be close to zero. These measurements were repeated between three and six times to confirm the precision of the measurements, especially since it was expected that the radial component would be higher in the impeller region as opposed to other regions of the vessel. By contrast, the CFD-predicted radial velocities on these three iso-surfaces were found to be higher than the LDV measurements, although still relatively small (10% of the tip speed). On the iso-surface at $z = -6.75$ mm, the predicted radial velocities were found to be positive, indicating that the flows points towards the vessel wall. On the iso-surface at $z = -15.75$ mm, the predicted radial velocities turned from positive ($0.63 < 2r/T < 0.9$) to negative ($2r/T > 0.9$) when moving close to the vessel wall, and for the iso-surface at $z = -25.75$ mm, the predicted radial velocities varied from about zero for $2r/T < 0.6$ to negative for $2r/T > 0.6$, which is counterintuitive. This confirms that the flow in an unbaffled vessel, especially when complex interactions between the impeller and the vessel are at work, as in Apparatus 2, is very different from that in a baffled system, even in the impeller region. The non-dimensional, CFD-predicted, radial velocities profiles were found to be nearly identical for $z = -6.75$ mm and $z = -25.75$ mm. However, for $z = -15.75$ mm, the CFD simulations showed that increasing the agitation speed results in a decrease in the relative radial velocities, when the radial velocities are positive.

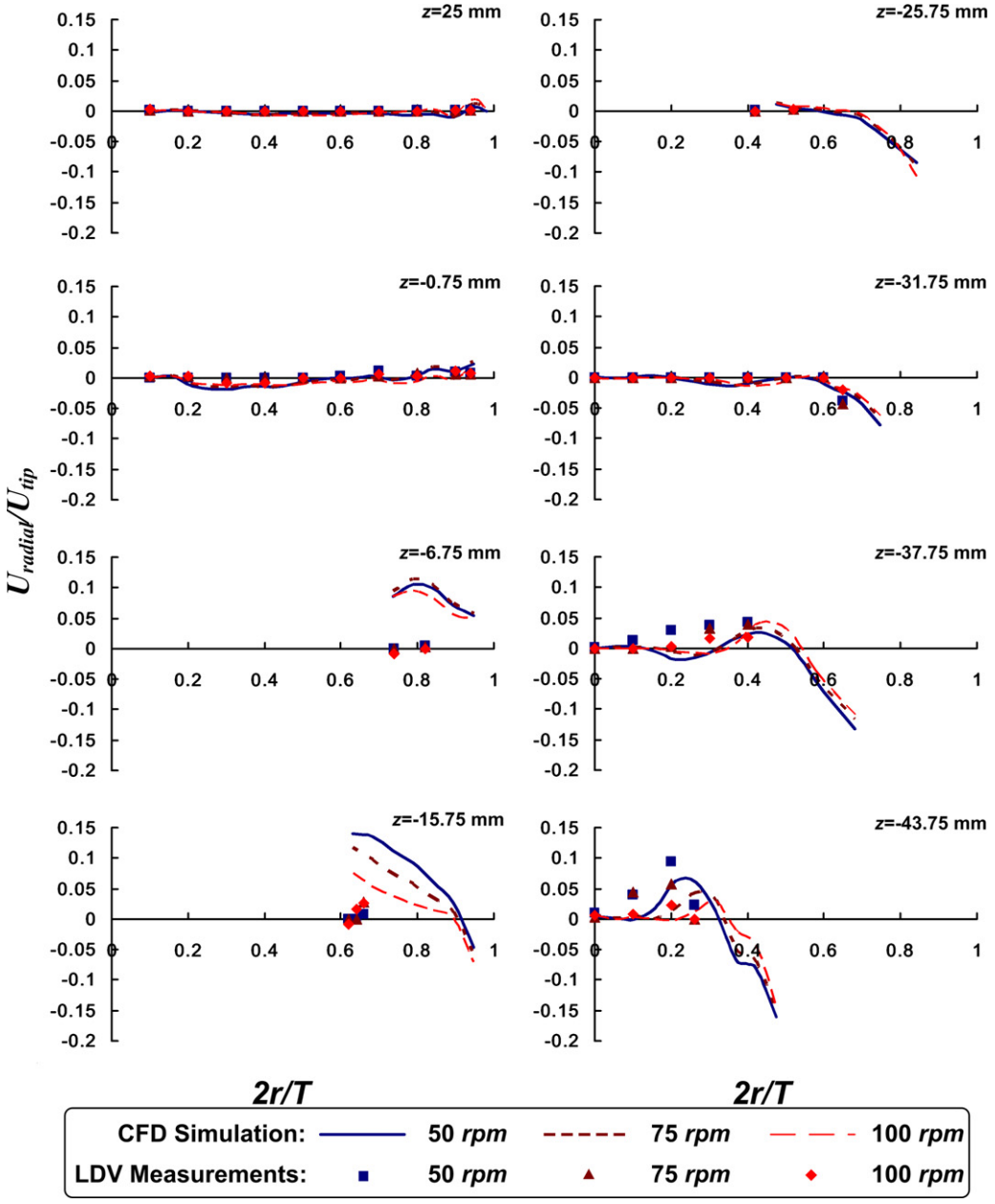

Fig. 5. Comparison between LDV data and CFD predictions for radial velocities on different iso-surfaces at agitation speeds of 50, 75 and 100 rpm.

4.1.3. Velocity profiles below the impeller

The tangential velocity profiles for the iso-surfaces below the impeller (at $z = -31.75$ mm, $z = -37.75$ mm and $z = -43.75$ mm) presented in Fig. 3 show that the non-dimensional velocities increase nearly monotonically with radial distance up until nearly the wall (*remark*: for these iso-surfaces the vessel wall is not found at $2r/T = 1$, as in the cylindrical section of the vessel, but at $2r/T < 1$ because of the curvature of the hemispherical vessel bottom). All the tangential velocity profiles in this region show a distinct pattern. In the inner core region (for $2r/T < 0.2$ for the iso-surfaces at $z = -31.75$ mm and $z = -37.75$ mm and for $2r/T < 0.3$ for the iso-surface at $z = -43.75$ mm) the non-dimensional tangential velocity starts at about 0 and increases linearly with the radial distance, thus making the fluid move in a solid-body type or rotation, at least in the tangential direction. In this region there is very good agreement between the LDV data and the CFD predictions, and the non-dimensional profiles are independent of rotational speed. In the outer region, the non-dimensional velocity still increases to eventually reach a maximum, but not as steeply as in the core region, and some, although small, differences among the curves at different agitation speeds can be noticed. For the profile near the vessel bottom ($z = -43.75$ mm), the core region extends almost up to the wall, making the fluid in this region swirl around the center line, where the velocity is zero or very close to it.

The velocity profiles for the same iso-surfaces reported in Fig. 4 show that the non-dimensional axial velocities are weak and generally positive, i.e., generating an upward flow below the impeller blade, while they become negative, implying a downward flow, only near the wall. It is interesting to notice that in the smaller inner core region, for $2r/T < 0.1$, both the LDV data and the CFD predictions indicate that the axial velocity is essentially zero irrespective of agitation speed and z value, and that it becomes slightly stronger only when $2r/T > 0.1$. The CFD prediction at the iso-surface at $z = -43.75$ mm, and to a more limited extent, the corresponding LDV data, show that outside this inner core region, there is a detectable surge in the upward velocity, which appears to be more

pronounced at lower agitation speeds. This phenomenon creates a weak but clearly detectable vertical recirculation loop. Although the CFD simulations over predict the experimental LDV velocity magnitudes, the flow pattern below the impeller is similar in both cases.

As for the radial velocities below the impeller, on the iso-surface at $z = -31.75$ mm in Fig. 5, the non-dimensional radial velocities are very close to zero for $2r/T < 0.6$, independently of the change in agitation speed. Negative velocity values near the vessel wall from both the LDV data and CFD simulations indicate that the radial velocity points slightly inward in this region. On the iso-surface at $z = -37.75$ mm, the axial velocities predicted by the CFD simulation are weakly inward while the LDV measurements show weakly outward velocities for $0.1 < 2r/T < 0.3$. The LDV measurements on this iso-surface show that the non-dimensional radial velocities decrease as the impeller agitation speed increases. On the iso-surface at $z = -43.75$ mm, peaks in the non-dimensional radial velocities appear at $2r/T = 0.2$, based on the LDV measurements. The peak values decrease as the impeller agitation speed increases. The peak radial velocities obtained from CFD simulation under predict the experimental data at impeller agitation speeds of 50 and 75 rpm. However, both the CFD and LDV results show a similar flow pattern in this region. It should be remarked that, similar to the axial velocity case, a small inner core region exists for $2r/T < 0.1$ where the radial velocity is extremely small irrespective of agitation speed and z value.

5. Velocity vectors and velocity magnitude

Having validated the CFD velocity predictions with LDV data, it is now possible to use CFD to examine the overall flow patterns generated in the Apparatus 2 vessel. Fig. 6 presents the velocity vectors generated by the CFD simulations on a vertical cross section through the impeller shaft for two different orientations of the impeller (i.e., on the y-plane, parallel to the impeller blade, and on the x-plane perpendicular to the impeller blade) at different impeller agitation speeds. The red color in the vector plots represents velocity magnitudes that are 0.2 m s^{-1} or higher. In all cases, the horizontal radial jet generated by the impeller produces weak upward and downward flows once it impacts the vessel wall, forming secondary recirculation loops above and below the impeller. However, the vertical location of the stagnation point where the radial jet impacts the vessel wall increases with the impeller agitation speed. Above the impeller, the circulation loops are dominated by weak axial velocities for all agitation speeds, with relatively poor top-to-bottom recirculation.

The flow pattern below the impeller is the most complex of the entire vessel and can be better observed in Fig. 7, which presents an expanded view of the velocity vectors near the vessel bottom. Two regions can be identified below the impeller based on the flow patterns associated with them. The first region is the outer region characterized by recirculation loops formed by the downwards flow originating from the radial jets produced by the agitation of the impeller near the vessel wall. The second region is the inner core zone just below the shaft at the center of the vessel bottom. This is the most important region in the dissolution vessel since the dissolving tablet is typically located in this region during most tests. This region is not penetrated by the downflowing recirculation loops of the first region, and it is clear from Fig. 7 that the flow in this central inner core region is very weak, variable, and unstable. Furthermore, this region appears to be a common feature of the flow pattern in the vessel independently of the agitation speed. This inner core region contracts (y-planes) and expands (x-planes) as the impeller rotates, and this expansion of this region suppresses the two circulation loops below the impeller.

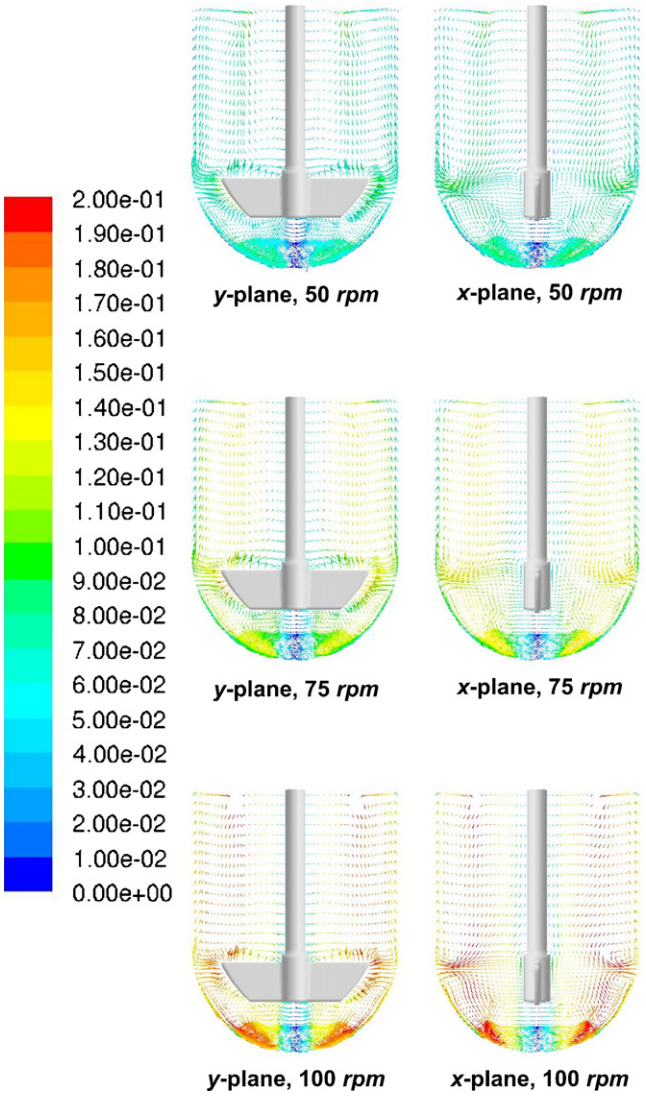

Fig. 6. CFD predictions of velocity vectors colored by velocity magnitude on a vertical cross section through the impeller shaft at different agitation speeds (50 rpm, 75 rpm and 100 rpm) and for different impeller orientations (y-plane: plane of the impeller blades; x-plane: plane perpendicular to the impeller blades). Red color represents velocity magnitudes equal to, or higher than, 0.2 m s^{-1}. (For interpretation of the references to color in this figure legend, the reader is referred to the web version of the article.)

It is interesting to notice that the inner core region becomes larger when the impeller agitation speed is higher, which is somewhat counterintuitive.

The picture emerging from the velocity vector plots can be compared with that obtained by examining the contours of the CFD-predicted velocity magnitude, shown in Fig. 8, where the magnitude of the velocity at every point in the vessel is plotted on a vertical cross section through the impeller shaft for different orientations of the impeller at different impeller agitation speeds. As before, the red color represents velocity magnitudes that are 0.2 m s^{-1} or higher. Above the impeller, the velocity magnitude increases significantly with increasing agitation speeds, except in the region near the shaft where the velocity is weaker. However, the velocity magnitude at each point in the vessel is equal to the square root of the sum of the squares of the three velocity components at that point. Therefore, the increase in velocity magnitude with agitation speed can be attributed, to a significant extent, to the corresponding increase in the tangential component, which is the dominating component of the velocity. A similar sit-

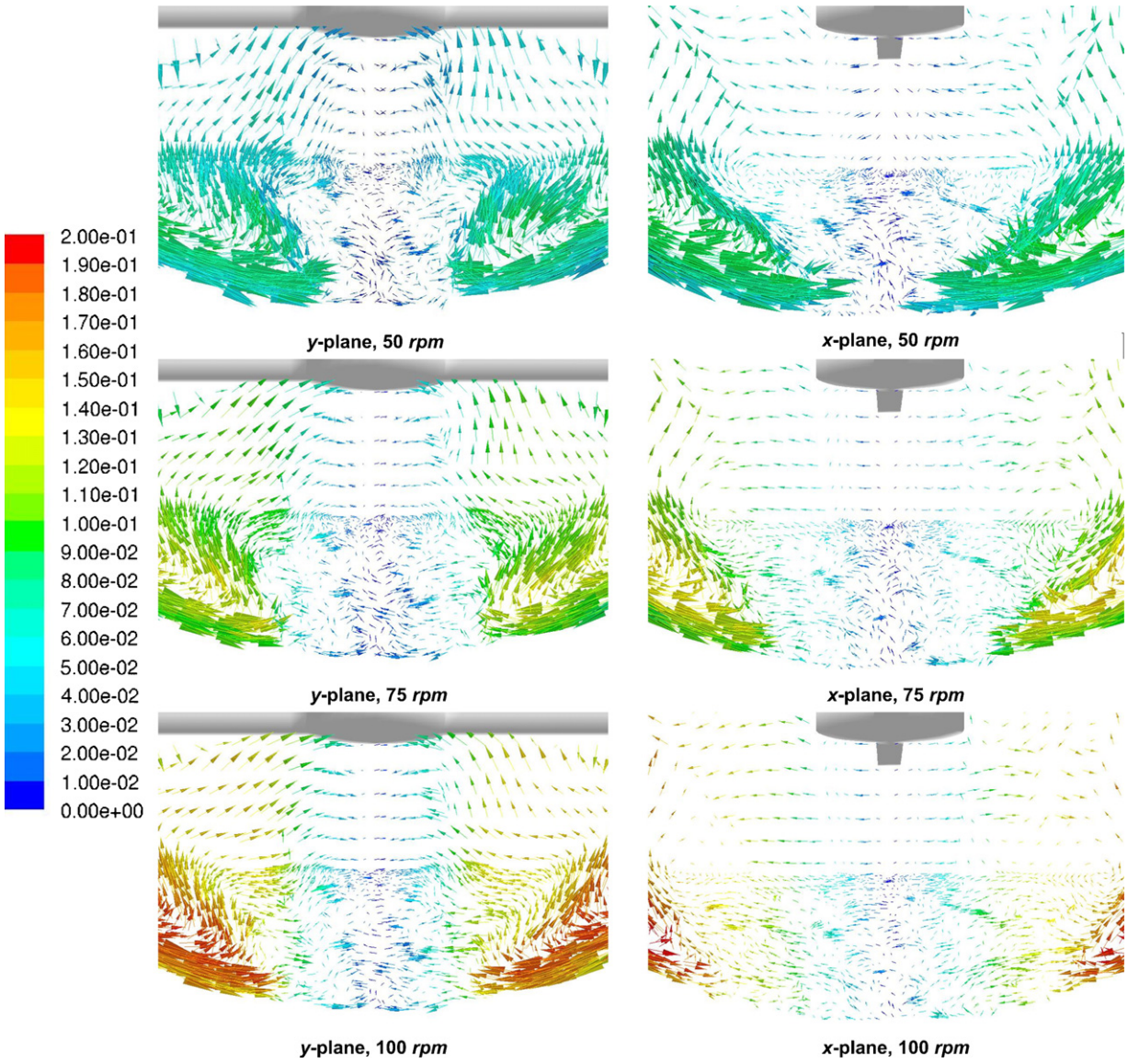

Fig. 7. CFD predictions of velocity vectors colored by velocity magnitude on a vertical cross section through the impeller shaft for the bottom region of vessel at different agitation speeds (50 rpm, 75 rpm and 100 rpm) and for different impeller orientations (*y*-plane: plane of the impeller blades; *x*-plane: plane perpendicular to the impeller blades). Red color represents velocity magnitudes equal to, or higher than, 0.2 m s^{-1}. (For interpretation of the references to color in this figure legend, the reader is referred to the web version of the article.)

uation can be observed in the region below the impeller. When the impeller agitation speed is increased, the velocity magnitude increases accordingly. However, in the inner core region below the shaft near the vessel bottom, the velocity is still very low velocity (blue color), even when the agitation speed is increased to 75 rpm or even 100 rpm. That is the region where the lowest velocity magnitudes in the entire vessel can be found, independently of the agitation speed. However, this is also the region where the tablet is typically located during a test.

5.1. Shear strain rate

In Fig. 9, the contour plots of the strain rate at 50 rpm, 75 rpm and 100 rpm are presented for different orientation of the impeller. Fig. 10 presents an expanded view of the strain rate contours near the vessel bottom. In these figures, the red color represents values of the strain rate that are 60 s^{-1} or higher. As one can expect, the high strain rate values are adjacent to both the impeller and the bottom vessel wall, since large velocity gradients occur in these areas. Fig. 9 shows that higher impeller agitation speeds result in a thicker and higher-strain rate layer (red color) next to the impeller blades. A higher impeller agitation speed also results in higher strain rate values above the top edge of the impeller. At 75 rpm the low strain rate area (dark blue color) appears to be much more extensive above the impeller compared to 50 rpm agitation speed case. However, when increasing the impeller agitation speed from 75 rpm to 100 rpm, this effect is not as obvious. Higher or lower strain rates in this region are not as critical to dissolution testing as the strain rates in the bottom region, where the tablet and most of its fragments typically are. Fig. 10 shows that increasing the impeller agitation speed decreases the low strain rate areas (dark blue) below the impeller, while producing a thicker and higher strain rate layer (red and yellow color) along the vessel bottom. At the same time, the high strain rate regions along the vessel bottom become more extended towards the bottom center. However, even at the 100 rpm, there is a region near the center bottom (where the tablet typically sits) in which the strain rate is low. In addition, there is a substantial difference between the strain rate at the very center of the vessel

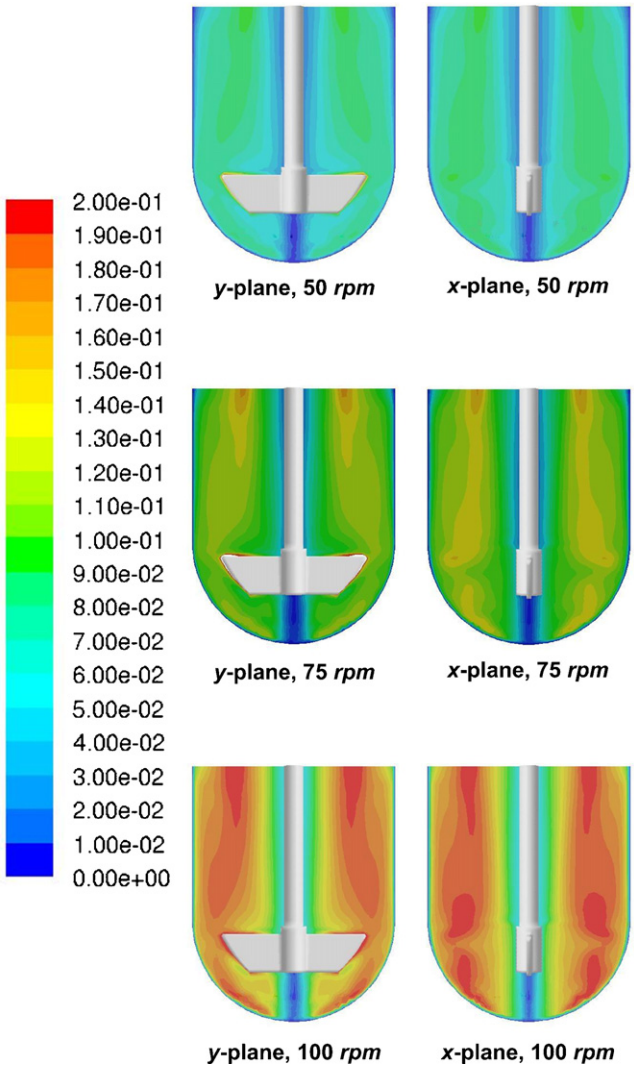

Fig. 8. CFD predictions of the velocity magnitude on a vertical cross section through the impeller shaft for the bottom region of vessel at different agitation speeds (50 rpm, 75 rpm and 100 rpm) and for different impeller orientations (*y*-plane: plane of the impeller blades; *x*-plane: plane perpendicular to the impeller blades). Red color represents velocity magnitudes equal to, or higher than 0.2 m s^{-1}. (For interpretation of the references to color in this figure legend, the reader is referred to the web version of the article.)

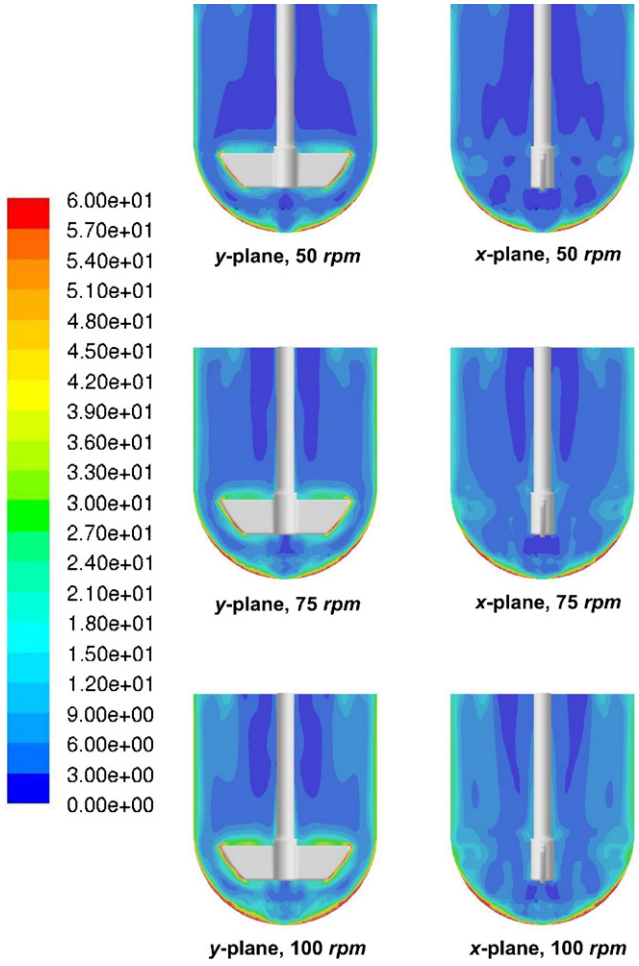

Fig. 9. CFD predictions of strain rates on a vertical cross section through the impeller shaft for the bottom region of vessel at different agitation speeds (50 rpm, 75 rpm and 100 rpm) and for different impeller orientations (*y*-plane: plane of the impeller blades; *x*-plane: plane perpendicular to the impeller blades). Red color represents strain rates equal to, or higher than, 60 s^{-1}. (For interpretation of the references to color in this figure legend, the reader is referred to the web version of the article.)

bottom (green or pale blue color) and the strain rate outside this center core area (red and yellow color).

6. Discussion

The results presented in this work show that the LDV experimental method used here is able to capture the details of the flow in Apparatus 2, including those relevant to the zone where tablet dissolution takes place. In addition, there is in general a significant overall agreement between the numerical CFD predictions and the experimental LDV data, and not just for the larger tangential velocities, but also for the axial and radial components, which are more difficult to measure because of their low values and the instabilities of the flow below the impeller bottom.

The experimental validation of the CFD approach implies that CFD can be effectively used to predict the hydrodynamics of Apparatus 2, visualize the three-dimensional velocity field in the apparatus, and draw general conclusions about the flow field. In practice, the main value of CFD lies in the large amount of information that it can generate and that cannot be obtained by experimentation, as with LDV measurements. In this work this means that once the CFD simulation has been completed (and validated), the hydrodynamic information anywhere inside the Apparatus 2 can be extracted and presented in a variety of forms, such as velocity vector plots or strain rate plots (Figs. 6–10). LDV measurements can only provide time-averaged velocities at the measurement point, but not transient velocities, such as those resulting from the impeller rotation, which occurs rapidly: for example, changes in the impeller position from the *y*-plane to the *x*-plane in Figs. 8–10 occur in 0.3, 0.2 and 0.15 s for impeller agitation speeds of 50, 75 and 100 rpm, respectively. The change in the hydrodynamics in such short periods of time cannot be captured by LDV measurements but can be predicted by CFD simulation. Hence, CFD can be applied to the study of the hydrodynamics in Apparatus 2 in a more efficient manner compared to LDV measurements.

Despite the wide use of Apparatus 2 in the pharmaceutical industry and its apparent simplicity, the results presented here show that the hydrodynamics in this apparatus is quite complex at any agitation speed. The three-dimensional flow pattern in the Apparatus 2 vessel can be obtained at different impeller agitation speeds using the information in CFD-generated Figs. 6–8, combined with the information from Figs. 3–5.

The flow patterns observed and those predicted for Apparatus 2 are generally very similar to each other for all agitation

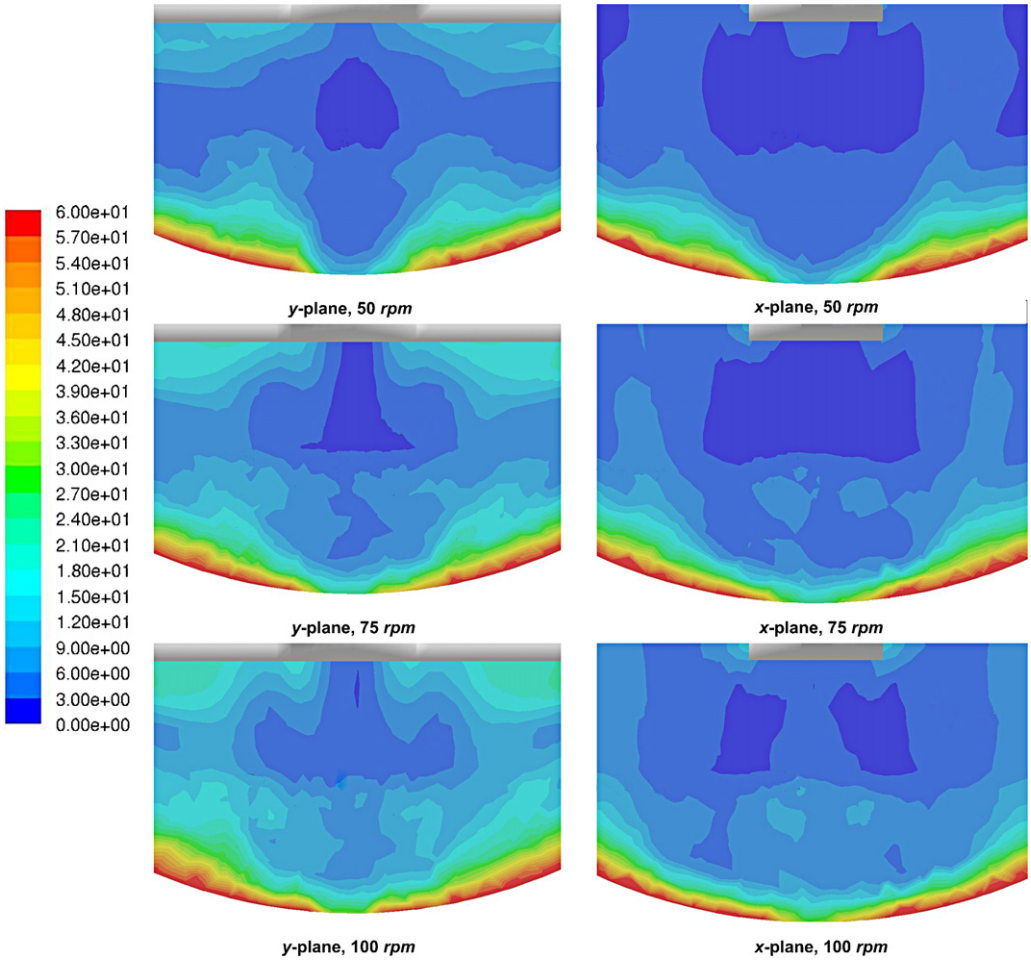

Fig. 10. CFD predictions of strain rates on a vertical cross section through the impeller shaft for the bottom region of vessel at different agitation speeds (50 rpm, 75 rpm and 100 rpm) and for different impeller orientations (*y*-plane: plane of the impeller blades; *x*-plane: plane perpendicular to the impeller blades). Red color represents strain rates equal to, or higher than, 60 s^{-1}. (For interpretation of the references to color in this figure legend, the reader is referred to the web version of the article.)

speeds (Figs. 6–8). Clearly, the tangential velocity component is the dominant flow feature in Apparatus 2 at all agitation speeds. The experimental data and the theoretical predictions both show that the largest values of the tangential velocities on all the iso-surface investigated in this work are between 40% and 50% of the impeller tip speed. In the upper portion of the vessel, this value of the tangential velocity extends over a significant portion of the radial coordinate, thus forming a "velocity plateau" region (iso-surfaces as $z = 25$ mm and -0.75 mm in Fig. 3), whereas near the vessel bottom the tangential velocity reaches a sharp peak at $2r/T \approx 0.4$ (bottom right panel in Fig. 3). The results presented in this figure additionally show that the non-dimensional velocity profiles at different agitation speeds are typically remarkably similar to each other, implying that the tangential velocities scale up very well with the impeller agitation speed. This is especially true for the lowest of the iso-surfaces investigated here (at $z = -43.75$ mm; last panel in Fig. 3). The close similarity of the non-dimensional curves in this region implies that increasing the impeller agitation speed results in a direct and proportional increase in the tangential flow below the impeller.

Compared to the tangential velocities, both the axial flow and the radial flow are typically much weaker in terms of magnitude, irrespective of impeller agitation speed and location within the vessel (Figs. 4 and 5). In general, radial velocities are even weaker than axial velocities: the highest axial velocity obtained by LDV measurements is about 15% of the impeller tip speed (50 rpm; iso-surface at $z = -0.75$ mm; Fig. 4) and the highest radial velocity obtained by LDV measurements is only about 10% of impeller tip speed (50 rpm; iso-surface at $z = -43.75$ mm; Fig. 5). However, the typical axial and radial velocities are much smaller than these peak values, confirming that Apparatus 2 is a relatively poor mixing device in the axial and radial directions at any impeller speed, as also previously reported (Bai et al., 2007a).

Figs. 4 and 5 show that the axial and radial velocities also scale up relatively well with impeller agitation speed. However, unlike the tangential velocities, higher impeller agitation speeds often produce slightly lower dimensionless axial and radial velocities on most iso-surfaces, indicating somewhat weaker relative flows in these directions. This implies that increasing the impeller speed does not translate into proportionally higher axial and radial velocities.

Because of its impact on the dissolution process, the effect of increased impeller speeds on velocity variations in the axial and radial directions near the bottom of the vessel needs to be examined more closely. The most striking feature of the flow in this region is that the inner core region below the impeller, for $2r/T < \sim 0.1$ (dark blue colored region in Fig. 8), persists even as the impeller agitation speed increases, although its size changes with impeller position (larger in *y*-plane and smaller in *x*-plane) and is inversely proportional to the impeller agitation speed. In the inner core region, increasing the agitation speed has a negligible effect on the relative axial as well as radial velocities (panel for $z = -43.75$ mm in Figs. 4 and 5). For the latter velocity component, the LDV data seem to indicate that the non-dimensional radial velocity actually

decreases with increasing impeller speeds in this region, implying that even doubling the agitation speed from 50 to 100 rpm would not change the absolute value of the radial velocity near the vessel bottom for $2r/T < 0.1$.

The velocity magnitude (equal to the square root of the squares of all three velocity components) outside the lower inner core increases as the impeller agitation speed increases, as indicated by the color change (from blue-green to yellow to red in Figs. 7 and 8). However, the length of the velocity vectors outside the center inner core region in Fig. 7 decreases as the impeller agitation speed increases. This indicates that below the impeller and outside the center inner core region, the tangential flow becomes more dominant at higher impeller agitation speeds since the length of the velocity vector represents the projection of only the axial and radial component of the velocity on the vertical planes (there is no tangential component in this projection, obviously). CFD can be additionally used to interpret the flow pattern. The impeller rotation generates two secondary recirculation loops above and especially below the impeller. Fig. 7 shows that these two axial–radial loops actually decrease in flow intensity and size as the impeller agitation speed increases, and the zone dominated by the solid body rotation around the impeller shaft expands, confirming not only that at higher agitation speeds the tangential flow becomes even more dominant than at lower agitation speeds, but also that this occurs at the partial expense of the axial and radial flows. In the lower region of the vessel, the secondary loops generated by the impeller are not able to penetrate the inner core region at any agitation speed. In fact, they become somewhat weaker in the axial and radial directions (as indicated by the smaller sizes of the vector arrow in Fig. 7) because of the increased dominance of the tangential flow. The inner region dominated by low axial and radial velocities actually appears to *expand* rather than contract as the agitation speed is increased (Fig. 7).

Since the tablet is typically located in this inner core region, at first glance these results would hardly justify increasing the agitation speed to increase dissolution effects. However, three other factors need to be considered. The first is that the tangential velocity component *increases* linearly with radial distance everywhere in the vessel, including in the inner core region below the impeller (panel for $z = -43.75$ mm in Fig. 3). This implies that the thickness of the boundary layer surrounding a non-disintegrating tablet in this region can be expected to decrease with increasing agitation speeds, resulting in an increase in the mass transfer rate and a faster dissolution process. Additional evidence of this effect can be observed in Fig. 10, which shows that the central region of low shear strain rate indeed shrinks as the agitation speed increases. The second factor to be considered is that in the outside the inner core region, i.e., for $2r/T > 0.1$ (and especially for $2r/T \approx 0.3$), there is a small region where the non-dimensional axial and radial velocities values are similar at different agitation speeds, which means that increasing the agitation speed indeed results in an increase in the actual values of axial and radial velocity components in the fluid there. This, in turn, could have an impact on disintegrating tablets since the tablet fragments in this outer core region will be pushed a bit more strongly in the positive radial direction (i.e., outward) as the impeller speed is increased, where the axial velocity component (Fig. 4) would produce the necessary lift. However, and more importantly, in order for the fragments to move to this outer region they need to leave the inner core region first. Therefore, the third and more critical factor is that the increased tangential velocities generated everywhere when the agitation speed is increased can produce a stronger centrifugal force on the tablet fragments even when they are in the inner core region because of the density difference between the solids and the liquid. Flow instabilities and velocity fluctuations generated by the rotating impeller (as can be seen by comparing the velocity profiles on the *y*-plane and *x*-plane in Fig. 7) would also move particle fragments from the inner core region to the outer core region, where lifting can then occur because of the higher axial velocities, thus promoting particle suspension and possibly reducing or eliminating completely coning effects.

This analysis shows that the key to fragment suspension cannot be attributed to an increase in the axial and radial velocity components in the inner core region below the impeller as a consequence of increases in the agitation speed (Figs. 4, 5 and 7), but it is rather the result of an increase in the tangential velocity everywhere in the vessel (*including* the inner core region below the impeller), which translates into greater centrifugal forces on the solids and the possibility for them of "escaping" the quiescent inner core region, entering the outer region below the impeller, and *only then* becoming suspended. In other words, increasing the impeller speed does not appear to produce higher axial velocities in the inner lower core region of the vessel capable of lifting the tablet fragments, but it rather generates larger tangential velocities and flow instabilities which are indirectly capable of moving the solids from the inner core to the external region outside it, where the axial flow is higher (even at 50 rpm) and solid suspension can take place. Increasing the agitation speed is in fact the typical strategy used by operators to help suspending particles and eliminate coning, although the velocity profiles obtained here and this analysis shows that this effect is not as strong and as direct as one would anticipate.

It should be additionally remarked that the exact location of the tablet on the vessel bottom during dissolution testing is critical for the rate at which the process occurs, and can result in statistically significant different dissolution curves, as previously shown (Bai and Armenante, 2009). This phenomenon is expected to be even more acute if the agitation is increased, since the flow field in which the tablet is immersed can be even more different depending on whether the tablet lies in the inner core zone below the impeller or outside it.

Finally, the distribution of the shear strain rate along the vessel bottom during dissolution testing is also critical for the dissolution rate since the shear strain rate in this region is the driving force behind the dissolution of non-disintegrating tablets and for disintegrating tablets whose fragments are not fully suspended. Increasing the agitation speed has an interesting effect on strain rate. On the one hand, it obviously increases the strain rate outside the inner core region below the shaft (Figs. 9 and 10), and this can be expected to increase the mass transfer to a tablet, or to tablet fragments, outside the inner core region. As already mentioned, this effect is primarily caused by the general increase in the magnitude of the tangential velocities, which scales up very well with impeller speed almost everywhere in Apparatus 2 because of the absence of baffles to counteract the increased tangential flow. Additionally, Fig. 10 shows that the low strain rate inner core region shrinks with increasing agitation speeds. On the other hand, this low strain region still exists even at 100 rpm, and this implies that as the agitation speed is increased the shear strain distribution becomes even less homogeneous on the vessel bottom. This means that the exact location of the tablet (or portions thereof) during dissolution can be expected to be even more critical for the dissolution process at higher agitation speeds than it already is at 50 rpm, as it was shown before (Bai and Armenante, 2009). The only important mitigating factor is that flow instabilities can be expected to increase as well, thus promoting the redistribution of tablet material along the vessel bottom and its exposure to higher velocities (enhancing suspension) and higher shear strain (enhancing mass transfer).

7. Conclusions

The following conclusions can be drawn from this work:

(a) the LDV measurements and the CFD velocity predictions in Apparatus 2 are in substantial agreement with each other regardless of impeller agitation speed;
(b) the tangential velocity is the dominating velocity component in the hydrodynamics of the Apparatus 2 vessel at all impeller agitation speeds. At higher agitation speeds, the dominance of tangential flow is even more obvious;
(c) the non-dimensional velocity profiles and the flow patterns at different impeller agitations speed are generally very similar to each other in the Apparatus 2 vessel;
(d) the size of the secondary recirculation loops above the impeller decreases and the size of the solid body rotation zone around the impeller shaft increases when the impeller agitation speed increases;
(e) below the impeller, a central inner core region can be found where both axial and radial velocities are extremely low, regardless of the impeller agitation speed. The secondary recirculation loops below the impeller are not able to penetrate the central inner core region, where the axial and radial flows are typically weak but complex, irrespective of the impeller agitation speed;
(f) the distribution of shear strain rate along Apparatus 2 vessel bottom is not uniform, and a zone always exists just below the shaft where the strain rate remains very low, even when the impeller agitation speed is increased;
(g) the non-uniformity of shear strain rate distribution is expected to have an impact on the mass transfer rate, and hence the dissolution rate of a tablet, depending on where the tablet is located during the dissolution testing. Tablets located outside the inner core region are expected to dissolve much more rapidly than those located within that zone;
(h) the increase in tangential velocity magnitude resulting from higher agitation speeds is likely responsible for moving the tablet fragments from the inner core zone, where the solids are initially located during a dissolution test, to the surrounding region, where solids suspension can occur. Consequently, increasing the agitation speed can be an effective strategy to reduce or eliminate particle "coning" effects, promote particle suspension, and increase solid–liquid mass transfer and hence dissolution rate.

In conclusion, the hydrodynamics in Apparatus 2 vessel is very complex, especially below the impeller and in the center of the vessel bottom and this complexity may contribute to high variability in dissolution testing, even when the agitation speed is changed.

Acknowledgements

The authors would like to thank Philadelphia Mixing Solutions, Ltd., and especially Wojciech Wyczalkowski, for donating the fiber optic probe used in the LDV system.

References

Bai, G., Armenante, P.M., Plank, R.V., Gentzler, M., Ford, K., Harmon, P., 2007a. Hydrodynamics investigation of USP dissolution test Apparatus 2. J. Pharm. Sci. 96, 2327–2349.

Bai, G., Armenante, P.M., Plank, R.V., 2007b. Experimental and computational determination of blend time in USP dissolution testing apparatus II. J. Pharm. Sci. 96, 3072–3086.

Bai, G., Armenante, P.M., 2008. Velocity distribution and shear rate variability resulting from changes in the impeller location in the USP dissolution testing apparatus II. Pharm. Res. 25, 320–336.

Bai, G., Armenante, P.M., 2009. Hydrodynamic, mass transfer, and dissolution effects induced by tablet location during dissolution testing. J. Pharm. Sci. 98, 1511–1531.

Baxter, J.L., Kukura, J., Muzzio, F.J., 2005. Hydrodynamics-induced variability in the USP Apparatus 2 Dissolution Test. Int. J. Pharm. 292, 17–28.

Bird, R.B., Stewart, E.W., Lightfoot, N.F., 2002. Transport Phenomena. John Wiley & Sons, Inc., New York.

Bocanegra, L.M., Morris, G.J., Jurewicz, J.T., Mauger, J.W., 1990. Fluid and particle laser Doppler velocity measurements and mass transfer predictions for USP paddle method dissolution apparatus. Drug Dev. Ind. Pharm. 16, 1441–1464.

Cohen, J.L., Hubert, B.B., Leeson, L.J., Rhodes, C.T., Robinson, J.R., Roseman, T.J., Shefter, E., 1990. The development of USP dissolution and drug release standards. Pharm. Res. 7, 983–987.

Costa, P., Lobo, J.M.S., 2001. Influence of dissolution medium agitation on release profiles of sustained release tablets. Drug. Dev. Ind. Pharm. 27, 811–817.

Cox, D.C., Furman, W.B., 1982. Systematic error associated with Apparatus 2 of the USP dissolution test I: effects of physical alignment of the dissolution apparatus. J. Pharm. Sci. 71, 451–452.

Cox, D.C., Furman, W.B., Thornton, L.K., 1983. Systematic error associated with Apparatus 2 of the USP Dissolution Test III: limitation of calibrators and the USP suitability test. J. Pharm. Sci. 72, 910–913.

FDA, 1997. Guidance for Industry: Dissolution Testing of Immediate Release Solid Oral Dosage Forms.

Fruitwala, M.A., Dondeti, P., Alkhawam, E., Ahmed, S., 1998. Rationales in the development of dissolution testing for solid oral dosage forms—an industrial, biopharmaceutical and regulatory perspective. Clin. Res. Regul. Aff. 15, 187–207.

Gibaldi, M., Feldman, S., 1967. Establishment of sink conditions in dissolution rate determinations. Theoretical considerations and application to nondisintegrating dosage forms. J. Pharm. Sci. 56, 1238–1242.

Kamba, M., Seta, Y., Takeda, N., Hamaura, T., Kusai, A., Nakane, H., Nishimura, K., 2003. Measurement of agitation force in dissolution test and mechanical destructive force in disintegration test. Int. J. Pharm. 250, 99–109.

Kortejärvi, H., Malkki, J., Marvola, M., Urtti, A., Yliperttula, M., Pajunen, P., 2006. Level A in vitro–in vivo correlation (IVIVC) model with bayesian approach to formulation series. J. Pharm. Sci. 95, 1595–1605.

Kukura, J., Arratia, P.C., Szalai, E.S., Muzzio, F.J., 2003. Engineering tools for understanding hydrodynamics of dissolution tests. Drug Dev. Ind. Pharm. 29, 231–239.

Kukura, J., Baxter, J.L., Muzzio, F.J., 2004. Shear distribution and variability in the USP Apparatus 2 under turbulent conditions. Int. J. Pharm. 279, 9–17.

Mauger, J., Ballard, J., Brockson, R., De, S., Gray, V., Robinson, D., 2003. Intrinsic dissolution performance of the USP dissolution apparatus 2 (rotating paddle) using modified salicylic acid calibration tablets: proof of principle. Dissol. Technol. 10, 6–15.

McCarthy, L., Kosiol, C., Healy, A.M., Bradley, G., Sexton, J., Corrigan, O., 2003. Simulating the hydrodynamic conditions in the United States pharmacopeias paddle dissolution apparatus. AAPS Pharm. Sci. Technol. 4.

McCarthy, L., Bradley, G., Sexton, J., Corrigan, O., Healy, A.M., 2004. Computational fluid dynamics modeling of the paddle dissolution apparatus: agitation rate mixing patterns and fluid velocities. AAPS Pharm. Sci. Technol. 5.

Moore, T.W., Hamilton, J.F., Kerner, C.M., 1995. Dissolution testing: Limitation of USP prednisone and salicylic acid calibrator tablets. Pharmacopeial Forum 21, 1387–1396.

Qureshi, S.A., McGilveray, I.J., 1999. Typical variability in drug dissolution testing: study with USP and FDA calibrator tablets ad a marketed drug (glibenclamide) product. Eur. J. Pharm. Sci. 7, 249–258.

Qureshi, S.A., Shabnam, J., 2001. Cause of high variability in drug dissolution testing and its impact on setting tolerances. Eur. J. Pharm. Sci. 12, 271–276.

Qureshi, S.A., Shabnam, J., 2003. Applications of a new device (spindle) for improved characterization of drug release (dissolution) of pharmaceutical products. Eur. J. Pharm. Sci. 19, 291–297.

Ross, M.S.F., Rasis, M., 1998. Mega paddle—a recommendation to modify apparatus 2 used in the USP general test for dissolution (711). Pharmacopeial Forum 24, 6351–6353.

Shah, V.P., Gurbarg, M., Noory, A., Dighe, S., Skelly, J.P., 1992. Influence of higher rates of agitation on release patterns of immediate-release drug products. J. Pharm. Sci. 81, 500–503.

United States Pharmacopeia 31/National Formulary 26, 2008. General Chapter <711> Dissolution. 12601 Twinbrook Parkway, Rockville, MD 20852-1790, USA.